



Real-time embedded ECG anomaly detection system with comparative analysis of CWT-based transfer learning performance across electrode types

Wissem Kharzi ^a*, Nacera Meziane ^a, Hadjer Zairi ^a, Malika Kedir Talha ^a, Lotfi Madaoui ^a, Oussama Kerdjidj ^b

^a Department of Electrical Engineering, LINS Laboratory, University of Science and Technologies Houari Boumediene, BabEzzouar Algiers, 16111, Algeria

^b Center for Development of Advanced Technologies, Algiers, Algeria

ARTICLE INFO

Keywords:

Transfer learning
Dry electrodes
Continuous wavelet transforms
Real-time systems
Anomaly detection
Edge computing

ABSTRACT

Electrocardiogram (ECG) is an essential tool to diagnose cardiac anomalies. However, the inherent variability of ECG signals contaminated by the presence of noise and artifacts during extended monitoring may lead to misdiagnoses. Consequently, conventional gel electrodes worsen the issue by causing skin irritation and degrading signal quality due to intermittent contact loss. This study introduces a real-time dry electrodes based ECG diagnostic assistance system to improve patient comfort and maintain signal quality. It integrates transfer learning models with continuous wavelet transform (CWT) techniques to build a robust recognition model to extracts more detailed information than traditional time domain representations. This investigation provides a comprehensive benchmarking analysis, assessing various CWT wavelets and their impact on the performance of deep learning architectures, including InceptionV3, VGG16, VGG19, Xception, and EfficientNetB0. Two datasets support the analysis: the publicly available PTB Diagnostic ECG dataset, which includes normal and pathological classes, and a proprietary dataset designed to detect hardware anomalies. Finally, the findings show that the VGG19 model achieved an accuracy of 99.87% when deployed on a Jetson Nano board, demonstrating effective training and validation processes while minimizing latency and computational overhead.

1. Introduction

Electrocardiograms are fundamental physiological signals essential for evaluating the heart's electrical activity [1,2]. These signals not only provide a comprehensive assessment of cardiac function but also offer invaluable diagnostic information related to the circulatory and nervous systems [3,4]. In recent years, extensive research efforts have been dedicated to advancing robust and efficient methods for processing and interpreting ECG [5]. Given the critical importance of reliable, accurate, and precise diagnostics particularly in the early detection of cardiac pathologies which is paramount for preventing heart diseases, as they remain the leading cause of mortality [6], according to the World Health Organization (WHO), approximately 18.6 million individuals die from heart-related ailments each year, accounting for 31% of all global fatalities [7]. Moreover, recent data from the World Heart Federation¹ reveals that deaths from cardiovascular disease have surged by 60% globally over the past 30 years, emphasizing the urgent need for early detection and timely intervention.

Despite these alarming statistics, conventional ECG monitoring techniques have several significant limitations. First, traditional methods rely heavily on manual interpretation, a process that is time-consuming and prone to errors. This issue is particularly concerning when subtle yet clinically significant changes are obscured by noise or confined to the time domain (1D) [7,8]. To address these shortcomings, frequency-domain approaches such as the Fourier transform (FT) and hybrid time-frequency techniques have been employed to capture details that may be hidden in the time domain [5]. The second issue concerns conventional gel electrodes, which introduce additional challenges during extended monitoring sessions by affecting both patient comfort and signal quality. These electrodes require adhesives to stay attached to the skin, which, over time, can cause irritation and discomfort. Furthermore, perspiration can weaken the adhesive, leading to a loss of contact between the electrode and the skin. This results in signal degradation, potentially compromising the accuracy of ECG outcomes [9].

* Corresponding author.

E-mail addresses: kharziwisseme@hotmail.com (W. Kharzi), nac.meziane@gmail.com (N. Meziane), zairi_hadjer@yahoo.fr (H. Zairi), malikakedir@gmail.com (M.K. Talha), madaoui.lotfi@gmail.com (L. Madaoui), kerdjidoussama@gmail.com (O. Kerdjidj).

¹ <https://world-heart-federation.org/news/deaths-from-cardiovascular-disease-surged-60-globally-over-the-last-30-years-report/>

To solve these problems, this paper describes an all-in-one embedded system that combines signal acquisition, processing, and intelligent interpretation to speed up diagnostic processes and make them more accurate. Central to this system is the adoption of dry electrodes, designed to maintain sustained signal quality over extended durations. Their conductivity is further enhanced by perspiration at the electrode-skin interface, thereby reducing skin irritation commonly associated with gel electrodes [10]. These dry electrodes are connected to an STM32F103C8T6 microcontroller and an AD8232 analog front-end circuit, forming the ECG acquisition stage. Following this, the development of the classification model involved comprehensive benchmarking, evaluating various continuous wavelet transform (CWT), and assessing their impact on robustness across multiple transfer learning (TL) models to identify the optimal approach for two datasets. This method, supported by recent literature, demonstrates superior performance and effectiveness [1,4,8,11–13]. Subsequently, the selected combination was implemented on the hardware board, utilizing multithreading and multiprocessing techniques to enhance system speed, ensure non-blocking execution, and prevent data loss, thereby optimizing the performance of the real time embedded system.

The rest of the paper is structured as follows: Section 2 reviews related work. Section 3 outlines a detailed description of the proposed method. Section 4 follows with a presentation of the results, including a detailed analysis of the ablation experiment outcomes. Finally, the paper concludes with a summary of key insights and future perspectives.

2. Related work

To provide a comprehensive context for the current investigation, this section reviews existing research on the three main aspects of this study.

2.1. ECG acquisition using dry electrodes

Recent advancements in bioelectrical monitoring have spurred significant interest in dry electrode technologies as a promising alternative to conventional gel electrodes. Dry electrodes offer numerous benefits including ease of preparation, long term stability, and reusability while minimizing some of the limitations of gel based systems such as skin irritation, drying, and the need for frequent replacement. However, challenges remain for example, many dry electrodes struggle to achieve good signal quality when interfacing with hair-covered regions, and some designs introduce discomfort during extended use. One innovative approach to overcome these challenges is demonstrated by a conductive Velcro electrode (CVE) that leverages an elastic hook hair structure [14]. Unlike traditional flat surfaced AgCl or silver cloth electrodes, the CVE's microstructured hooks can penetrate hair to establish reliable contact with the skin while significantly reducing discomfort during prolonged wear. This electrode exhibits low impedance, a high signal to noise ratio, strong water and mechanical resistance, and maintains performance even after repeated washing and mechanical compression. In addition, the CVE has been successfully applied in applications such as electromyography-based gesture recognition, achieving accuracies above 90%. In another advancement aimed at improving ECG monitoring, researchers have developed a conformal and soft dry electrode using anisotropic conductive rubber [15]. Fabricated via screen and stencil printing processes, this electrode ensure comfortable and durable skin contact. Its performance stability over extended periods (up to 170 h) and under more than 1500 bending cycles further underscores its potential for long-term wearable applications. Parallel to these developments, significant progress has been made using 3D printing and bioprinting technologies. Abdou et al. [16] demonstrated that 3D printed dry electrodes can capture high quality ECG signals suitable for short term wireless monitoring, with heart rate estimations comparable to those of wet electrodes.

Further work by the same group [17] expanded on this by introducing three electrode designs stiff, soft/flexible, and fabric based to address different application needs stiff materials for short term acquisition and soft or fabric materials for longer term, wearable monitoring. Wang et al. [18] introduced an elastic dry electrode designed for real-time ECG acquisition from the palm, which obviates the need for conductive paste by reducing skin impedance without penetrating the cuticle layer a notable benefit for continuous monitoring during everyday activities and in challenging environments. Complementing these efforts, a comparative study [19] evaluated motion artifact resistance among various dry electrode materials. Their results highlighted that solid electrodes made from materials such as stainless steel and platinum exhibit higher signal-to-noise ratios and lower skin-electrode impedance than their porous counterparts, making them better suited for both stationary and ambulatory applications. Lastly, Early studies demonstrated that Orbital electrodes perform comparably to commercial wet electrodes [20], and more recent investigations attribute their high performance to a design that enables deeper penetration into the upper skin layer. This feature not only reduces susceptibility to movement artifacts but also improves overall signal fidelity a key factor in long term monitoring applications [21]. Building upon these insights, our work leverages the proven advantages of the Orbital design, aiming to optimize electrode functionality for sustained use in clinical and research settings.

2.2. Identifying and classifying ECG anomalies

Various approaches have been developed to detect heart anomalies, each offering distinct advantages and limitations. This section reviews key methods in ECG signal processing and classification. One hybrid method combining DWT and Principal Component Analysis (PCA) [22] was proposed to enhance cardiac condition detection using the PhysioNet database, by extracting features and applying an Adaptive Neuro-Fuzzy Inference System (ANFIS) classifier, this method achieved high classification accuracy with excellent sensitivity and specificity. A comprehensive review from 2019 to 2024 highlights the effectiveness of deep learning (DL) techniques in ECG classification [23]. Leveraging large datasets, DL models successfully extract hidden features, leading to robust performance in heart anomaly detection. Another study [24] classified ECG beats with 94.6% balanced accuracy on the MIT-BIH arrhythmia database using Convolutional Neural Networks (CNNs) with fine-tuning pre-trained networks demonstrated the strength of TL for ECG anomaly detection. Maleki et al. [25], explored the efficacy of wavelet transformation combined with machine learning classifiers, such as K-Nearest Neighbors and Support Vector Machines, for ECG classification across cardiovascular conditions on the MIT-BIH Arrhythmia Database showing promising results, emphasizing the potential of wavelet-based feature extraction in medical diagnostics. A fusion model combining CNN, LSTM, and Transformer architectures enabled comprehensive feature extraction, achieving superior classification performance. Tests on the MIT-BIH arrhythmias database demonstrated that this hybrid approach outperformed prior models, setting a new standard for accuracy [8].

In summary, findings indicate that the combination of CWT and deep learning shows excellent diagnostic potential, warranting further exploration and optimization.

2.3. Real time detection using advanced boards

The selection of appropriate hardware components is vital for enhancing and concretizing the ECG monitoring software system, where accuracy, speed, and reliable outcomes are paramount. Several studies have investigated diverse approaches to improve ECG monitoring, emphasizing low power consumption, portability, and advanced data processing methods. A notable study [26] presented a low-power wireless system designed to predict early signs of sudden cardiac arrest,

using an optimized convolutional neural network (CNN) model implemented on the NVIDIA Jetson achieved an accuracy of 89% in identifying irregular heartbeats, with a normal beat classification F1 score of 0.94 and a ROC score of 0.886 demonstrating strong performance. Another approach [27] involves an FPGA-based platform for real-time ECG signal diagnosis acceleration. This platform compresses data using linear approximation to speed up diagnosis and reduce memory usage, achieving a 71% reduction in execution time compared to processor-only systems. Pramukantoro et al. [28] conducted a comparative analysis of classification features for ECG signal classification on Raspberry Pi, evaluating various feature extraction techniques using wearable sensor data. This study identified the most discriminative features and their impact on classification performance, highlighting the trade-offs between computational complexity and accuracy. The findings support the development of efficient, accurate, wearable-based ECG monitoring systems. Furthermore, Mhamdi et al. [29] utilized deep learning models to diagnose COVID-19 contamination based on ECG images. Using convolutional neural networks (MobileNetV2 and VGG16), these models achieved excellent classification rates, aiding in the quick and efficient diagnosis and prediction of abnormal cardiac activities due to SARS-CoV-2 virus contamination.

These outcomes highlight the significant advantages of implementing real-time ECG classification systems on optimized hardware, including enhanced diagnostic efficiency and responsiveness. Leveraging embedded platforms with deep learning models enables timely and accurate detection.

3. Proposed method

The proposed system, illustrated in Fig. 1, consists of four primary stages. The ECG acquisition and signal processing stage employs dry electrodes combined with a high-speed, cost-effective microcontroller to execute signal processing tasks with minimal signal attenuation, thereby preserving the integrity of the acquired data. Next, the process moves to the ECG conversion stage, where various CWT wavelets are applied to ECG datasets. These transformations facilitate the generation of scalogram representations, which are suitable for subsequent classification tasks. The output from this stage transitions seamlessly to the model evaluation stage, where these scalograms are analyzed using different TL models to compare their classification performance. This comparative analysis helps identify the optimal model for the system. Finally, the deployment stage builds on the results from the evaluation stage by implementing the best performing model on an embedded board with a robust architecture, ensuring the system's practical applicability and reliability.

3.1. ECG acquisition and signal processing stage

The acquisition stage is a critical component of the system, while poor signal recordings can lead to multiple operational issues. Therefore, it is essential to enhance the recording quality and minimize artifacts, meanwhile maintaining a compact and cost-effective design. To address these requirements, an optimized acquisition system consisting of three parts is proposed.

(a) Electrode select and placement: In this application, the Orbital SilverBumps® dry electrodes [30] were chosen for their unique surface design, which allows bioelectric signal measurement without gels or adhesives. These dry electrodes offer several advantages such as: they provide superior signal quality exhibiting improved signal to noise ratios, reduced motion artifacts and enhance patient comfort during extended monitoring sessions. In a clinical study, the incidence of skin irritation with traditional gel electrodes was reported to be approximately 8.7% over 48 h of continuous use, Whereas Orbital SilverBumps® dry electrodes demonstrated a significantly lower rate around 2.3%. FDA cleared for continuous, single patient ECG use for up to 48 h, the SilverBumps® electrodes are arranged in a three-electrode

configuration. Two electrodes, placed on the subject's arms, capture the cardiac signal, while a third electrode on the right leg serves as the reference, as shown in Fig. 1.

(b) Amplification and analog filtering: The AD8232 module is a compact ECG signal conditioning block (4×4 mm) that amplifies the electrical signals captured by surface electrodes.² It features an integrated instrumentation amplifier combined with a two-pole high-pass filter. The high-pass filter attenuates low-frequency noise components such as baseline wander, motion artifacts, and electrode half-cell potentials, thereby ensuring that the amplified signal accurately represents the cardiac activity [31,32]. To further enhance signal quality and avoid aliasing during analog to digital conversion, an external passive RC low-pass filter is implemented. This filter is designed with a cutoff frequency $F_c = F_s/2 = 250$ Hz where ($F_s = 500$ Hz) is the sampling frequency of the STM32 microcontroller. Consequently, the RC low-pass filter attenuates frequencies exceeding the Nyquist limit ($F_s/2$), effectively mitigating high frequency interference and preventing aliasing artifacts.

(c) Processing and recording: The output signal from the AD8232 is then connected to an ADC input of the STM32F103C8T6 ARM microcontroller [33]. It is recognized for its miniaturized dimensions (53x22.5 mm) and high-speed execution with a 72 MHz clock, rendering it appropriate for this application [34]. The sampling frequency is set to $F_s = 500$ Hz. Subsequently, we applied a fourth-order Butterworth low-pass filter due to its smooth frequency response and minimal phase distortion, followed by a notch filter to remove 50 Hz power line noise. These procedures have significantly improved the quality of the ECG signal by reducing noise and interference while preserving the relevant cardiac information. The obtained data was recorded in .CSV format through UART communication via a USB connection to a computer, enabling the creation of a dataset.

3.2. ECG signal conversion stage

In this phase, ECG data is transformed into scalogram format, to enable more effective feature extraction and analysis. This process involves a thorough description of the datasets, alongside a detailed explanation of the conversion mechanism and their resulting outcomes.

3.2.1. Datasets description

Careful selection of datasets is essential to ensure accurate results and optimal performance in ECG analysis. Since ECG signals are highly sensitive to anomalies whether due to cardiac conditions or noise, we have chosen the PTB PhysioNet dataset, which includes a diverse range of diseases. In addition, we have recorded our own dataset, which is specifically designed to detect hardware anomalies caused by common noise sources that can affect signal quality.

- (a) Public dataset:** The PhysioNet PTB Diagnostic ECG Database [35] was selected primarily to distinguish between healthy ECG signals and those indicative of disease. It comprises recordings from 290 individuals, including both healthy subjects (class 0) and patients diagnosed with various cardiac conditions such as myocardial infarction, bundle branch block, and other conduction abnormalities, all grouped into the same class (class 1). This classification approach is widely used and has been adopted in numerous studies. For instance, Sadia et al. [8] presented their results using this method and compared them with those obtained by others. Although the PTB dataset includes multi-lead recordings with up to 15 leads (including the standard 12-lead configuration) at a sampling frequency of 1000 Hz, we specifically addressed certain considerations to align with our study's scope

² <https://www.analog.com/media/en/technical-documentation/data-sheets/ad8232.pdf>

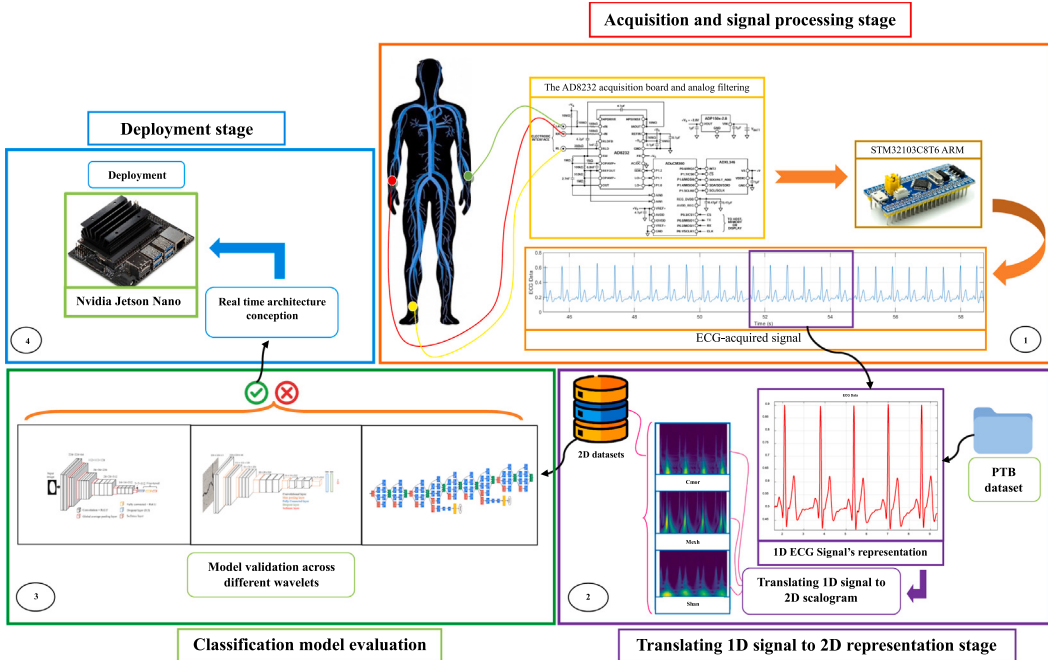


Fig. 1. Overview of the proposed system.

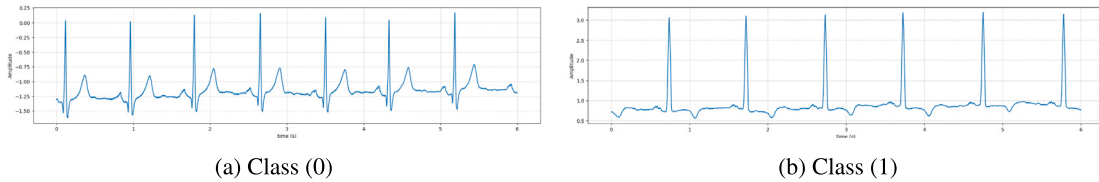


Fig. 2. Temporal domain representation of PTB signal classes with (a) Class (0) and (b) Class (1).

and ensure coherence with our proprietary dataset. As a result, we chose to utilize only Lead I and downsampled the data to 125 Hz, a value supported by previous studies [36].

Table 1 summary dataset classes and details and Fig. 2 shows an example signal for each class.

- (b) **Proprietary dataset:** Normal and Interference-Affected Records (NSIR Dataset) was recorded at the LINS Laboratory within the University of USTHB in Algeria using the designed system described previously, consist of 149 ECG signals recorded from healthy subject [37] divided in three classes. The main objective was to identify and differentiate **normal-recorded** ECG signals from those affected by two common types of interference according to the literature [5] referred as **The 50/60 Hz power line interference** and **electrode contact noise caused by unstable movement**. **Table 1** presents a breakdown of the dataset and Fig. 3 presents an example signal for each class, Moreover a complete guide how to use this dataset is available publicly.³

3.2.2. Continuous wavelet transform (CWT)

Various representations are viable, including time–frequency representations such as spectrograms, wavelet transforms, and scalograms [12,13,38]. in this study the scalogram representation based on CWT technique has been selected due to its well-established effectiveness in capturing both time and frequency characteristics simultaneously, making it invaluable for analyzing non-stationary signals, such as ecg [1, 11], Unlike Haar and Daubechies based wavelets approach, which

may overlook subtle signal details [39–41]. Furthermore this transform evaluates the similarity between an input signal $x(t)$ and various scaled and translated versions of a chosen wavelet function $\Psi(t)$ [1]. The CWT of a signal $x(t)$ is defined by the following equation (1):

$$CWT(a, b) = \frac{1}{\sqrt{|a|}} \int_{-\infty}^{\infty} x(t)\Psi\left(\frac{t-b}{a}\right) dt \quad (1)$$

Where, a and b are the scaling and translation parameters, respectively, and Ψ denotes the complex conjugate of the wavelet function. The parameter a controls the dilation (scaling) of the wavelet, allowing the analysis of different frequency components, while b shifts the wavelet in time, enabling the detection of temporal variations in the signal.

Moreover, The scalogram is a graphical representation of the CWT coefficients calculated with Eq. (2), which shows how the signal's energy is distributed across different scales and times. This provides a detailed view of the frequency content of a signal over time, making it easier to identify transient features and localized phenomena, particularly beneficial for ECG signals that often contain rapid changes in amplitude and frequency.

$$Scalogram(s, \tau) = |CWT(s, \tau)|^2 \quad (2)$$

Furthermore, it offers a wide options for selecting the mother wavelet function, each one with distinct properties suited to different signal characteristics [42]. This versatility enhances the classifier's capability to extract pertinent features, thereby bolstering its overall performance and robustness [1]. In this study, three types of wavelets were explored [43]: the Complex Morlet Wavelet (Cmor), the Mexican

³ <https://github.com/kharzi-wissem/ReadDryEcgData.git>

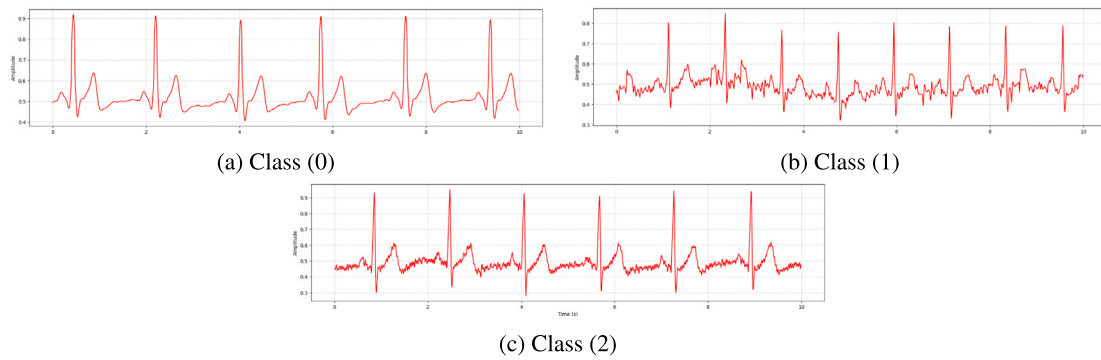


Fig. 3. Temporal domain representation of NSIR signal classes with (a) Class(0), (b) Class(1) and (c) Class(2).

Table 1
Summary of datasets classes and details.

Dataset	Class number	Type of record	Annotation	Number of records
PTB Dataset	Class 0	Healthy controls	Normal	35 (%)
		Myocardial infarction		
		Cardiomyopathy/Heart failure		
		Bundle branch block		
	Class 1	Dysrhythmia	Abnormal	65 (%)
		Myocardial hypertrophy		
		Valvular heart disease		
NSIR Dataset		Myocarditis		
		Miscellaneous		
		Total Records for PTB Dataset		549
	Class 0	Normal recorded ECG signals	N	28.1 (%)
	Class 1	Electrode contact noise	ECN	42.2 (%)
	Class 2	50/60 Hz power line interference	PLI	29.5 (%)
		Total Records for NSIR Dataset		149

Hat Wavelet (Mexh) known as the Ricker wavelet, and the Shannon Wavelet (Shan). These wavelet functions were implemented using the PyWavelets⁴ library in Python within the Visual Studio Code environment. Their mathematical expressions are presented in Eqs. (3).

$$\psi(t) = \frac{1}{\sqrt{\pi}B} \exp\left(-\frac{t^2}{B}\right) \exp(j2\pi Ct) \quad (a)$$

$$\psi(t) = \frac{2}{\sqrt[4]{3}\sqrt{\pi}} \exp\left(-\frac{t^2}{2}\right) (1-t^2) \quad (b)$$

$$\psi(t) = \sqrt{B} \frac{\sin(\pi B t)}{\pi B t} \exp(j2\pi Ct) \quad (c)$$

The Cmor wavelet, highlighted in the literature for its effectiveness in detecting and analyzing ECG signal frequency components due to its oscillatory nature, is particularly useful for capturing periodic and quasi-periodic features, making it ideal for heart rate variability analysis [44]. Similarly, the Mexh wavelet, which resembles the second derivative of a Gaussian function, excels in pinpointing QRS complexes due to its pronounced peak and zero-crossing properties, crucial for accurate R-peak detection and heart rate estimation [45]. Additionally, the Shan wavelet, known for its rectangular shape in the frequency domain, is adept at capturing abrupt changes and transient features in ECG signals, thus proving effective in identifying arrhythmias and other pathological conditions [46].

3.2.3. Conversion process and visualization

To demonstrate the effect of different wavelets on ECG signals, a specific protocol outlined in Fig. 4 is applied separately to each

dataset. Firstly, data is segmented into parts containing 10 PQRST complexes, which are treated as informational units. Each segment is then transformed using a distinct wavelet, creating three sub datasets per original dataset each reflecting a different mother wavelet.

Fig. 5 displays signals examples from the NSIR dataset (in red) and the PTB dataset (in blue) along with their 2D scalogram representations by applying the different wavelets. The columns represent Cmor, Mexh, and Shan wavelets, respectively.

In the left column, the CMOR wavelet effectively captures both low- and high-frequency components, resulting in broad high-energy regions that highlight essential ECG features, particularly around the R-peaks. This wavelet provides a detailed view of the entire ECG cycle, including the P, QRS, and T waves, making it ideal for a comprehensive representation of the ECG signal. In the middle column, the MEXH wavelet creates sharper, more localized high-energy regions, focusing primarily on the R-peaks and QRS complex. Its capacity to highlight rapid transitions makes it highly effective for isolating the QRS complex. However, it underrepresents lower-frequency elements, such as the P and T waves, when compared to the CMOR scalograms.

In the right column, the Shan wavelet concentrates high-energy regions around the R-peaks with precise localization, focusing on high-frequency features such as the QRS complex. However, it provides limited visibility of lower-frequency components like the P and T waves. Each wavelet brings unique insights into the ECG signal analysis. The CMOR wavelet offers a balanced, comprehensive view that spans both high- and low-frequency components, while the MEXH and Shan wavelets excel at highlighting the sharp transitions of the QRS complex, beneficial for QRS-specific analysis. Given the broader frequency range captured by the CMOR wavelet, it may support improved classification performance, especially when leveraging the complete ECG cycle.

⁴ <https://pywavelets.readthedocs.io/en/latest/ref/cwt.html>

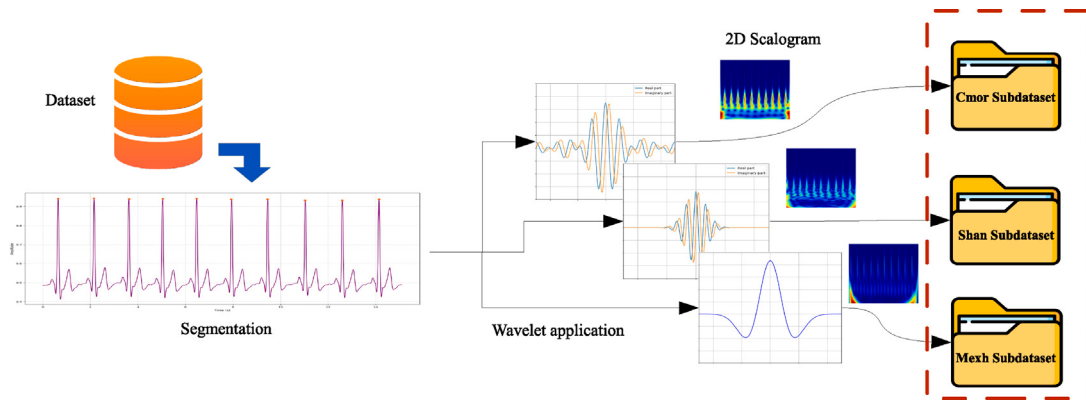


Fig. 4. Conversion process diagram and sub-datasets creation.

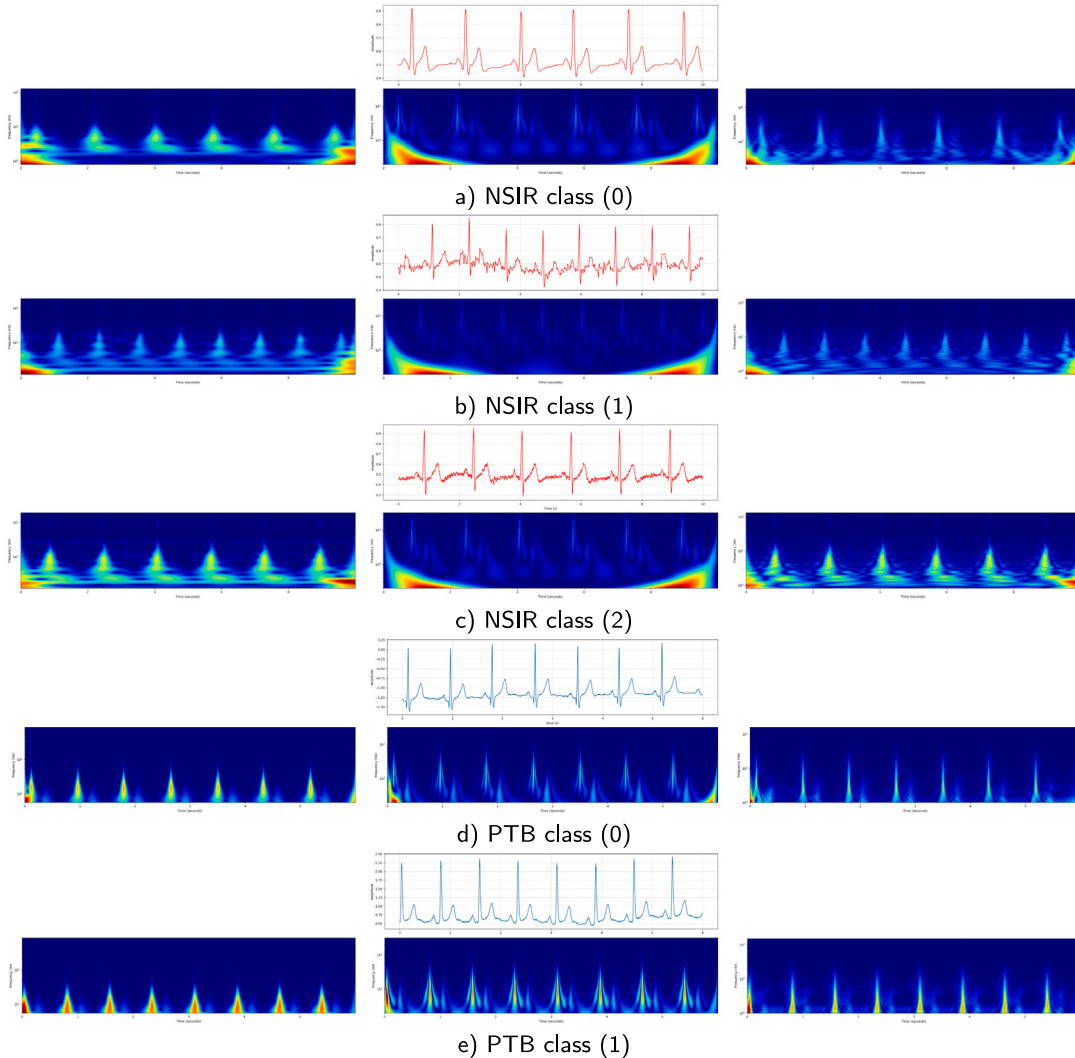


Fig. 5. Comparative analysis of ECG Signal scalograms representation, (a) Class 0 signal from SNIR along with 2D representation using CMOR, MEXH, and SHAN wavelets respectively from left to right, (b) Class 1 signal from SNIR along with 2D representation using CMOR, MEXH, and SHAN wavelets respectively from left to right, (c) Class 2 signal from SNIR along with 2D representation using CMOR, MEXH, and SHAN wavelets respectively from left to right, (d) Class 0 signal from PTB along with 2D representation using CMOR, MEXH, and SHAN wavelets respectively from left to right, (e) Class 1 signal from PTB along with 2D representation using CMOR, MEXH, and SHAN wavelets respectively from left to right.

Table 2
Summary of different architecture models.

Model	Input size	Parameters (Million)	Depth	Size (MB)	Advantages
Inv3 [48]	(299 × 299x3)	23.9	48	89	Optimized for speed and accuracy, requires GPU/TPU
Xce [49]	(299 × 299x3)	22.9	71	85	Uses depthwise separable convolutions, high computational resources
V16 [50]	(224 × 224x3)	138	16	515	Simple, high memory usage
V19 [50]	(224 × 224x3)	144	19	535	Higher capacity, even higher memory usage
Efb0 [51]	(224 × 224x3)	5.3	82	20	Efficient, suitable for edge devices, may have lower accuracy

3.3. Classification model evaluation stage

To validate the high effectiveness of using 2D scalograms in conjunction with transfer learning (TL) models, it is essential to delve deeply into which wavelets offer superior feature extraction capabilities when paired with TL models. To this end, each sub-dataset, generated from the conversion process, was used to train five deep learning models: InceptionV3 (Inv3), Xception (Xce), VGG16 (V16), VGG19 (V19), and EfficientNetB0 (Efb0) under varied parameters to identify the optimal configuration.

3.3.1. Transfer learning technique

TL is an approach in which a pre-trained model, initially trained on a large dataset, is adapted to a new, related task with a smaller dataset. This strategy leverages the model's learned features, significantly reducing training time and enhancing performance [47]. However, each selected TL model in this application differs in terms of architecture and parameters, as depicted in Table 2.

3.3.2. Experimental setup and configuration parameters

The experiments in this study were conducted using Visual Studio Code as the integrated development environment, with TensorFlow and Keras as the deep learning frameworks. The hardware setup consisted of a Windows 11 system with an Intel(R) Core(TM) i7-8565U CPU, 8 GB RAM, and an Nvidia Mx230 GPU with 6 GB memory, utilizing CUDA 11.3. Before initiating the training and validation processes, input images were resized to either (299 × 299) or (224 × 224), depending on the model requirements. The dataset was stratified using a fixed seed (37) into an 80% training set, with the remaining 20% evenly split between validation and testing, ensuring balanced class representation. For model training, we employed the Adaptive Gradient Descent (Adam) optimizer with two learning rates: the default $Lr = 10^{-3}$ and a fixed $Lr = 10^{-4}$, training over 50 epochs with a batch size of 64. Based on ImageNet, the base of each model was frozen to retain its learned representations, while only the newly added layers were fine-tuned for the specific classification task. The extended architecture builds upon this foundation by incorporating a global average pooling layer for dimensionality reduction, followed by a fully connected layer with 1024 units using ReLU activation to introduce non-linearity, and finally, a dense softmax layer that outputs predictions corresponding to the number of class labels.

The model's performance will be rigorously evaluated using key metrics: Precision (P), Accuracy (A), F1 Score (F), Recall (R), and Loss (L). Additionally, the model's effectiveness will be visually assessed through the Receiver Operating Characteristic (ROC) curve. The mathematical formulas for these metrics are provided in the Eqs. (4).

$$\begin{aligned} P &= \frac{TP}{TP + FP} & (a) \quad A &= \frac{TP + TN}{TP + TN + FP + FN} & (d) \\ F &= 2 \times \frac{Ps \times R}{Ps + R} & (b) \quad L &= \text{categorical cross-entropy} & (e) \\ R &= \frac{TP}{TP + FN} & (c) \end{aligned} \quad (4)$$

Where TP represents true positives, FP represents false positives, TN represents true negatives, and FN represents false negatives.

3.4. Deployment on the embedded board

Upon completing the conception and evaluation of the optimal TL model and identifying the most effective wavelet for ECG diagnosis, the model is deployed onto the Jetson Nano Developer Kit, which demonstrates strong performance suitable for this application.

3.4.1. Jetson Nano hardware specifications

The NVIDIA Jetson Nano Developer Kit⁵ is a powerful board designed for edge computing, enabling the deployment of AI models and real-time processing in a compact and energy-efficient form. With its 128-core Maxwell GPU, quad-core ARM Cortex-A57 processor, and 4 GB of LPDDR4 memory, it supports a wide range of AI tasks, from image recognition to natural language processing. Exploiting tools such as CUDA, cuDNN, and TensorRT. Furthermore, the board employs both multiprocessing and multithreading strategies to optimize computational efficiency. Through multiprocessing, the system can allocate tasks across multiple CPU cores, allowing parallel execution of processes essential for managing high computational loads and mitigating potential bottlenecks. On the other hand, multithreading subdivides a single process into multiple concurrent threads, enhancing task efficiency, particularly for operations with high I/O demands.

3.4.2. Real time system architecture

Fig. 6 illustrates the detailed structure of the system architecture, featuring an optimized parallel processing design that distributes functions for data acquisition, signal conversion, and classification across four primary cores. This parallelization enables simultaneous task execution, reducing latency and ensuring a fast and efficient prediction response. The process begins with importing the necessary software libraries and resources. Next, on the main core (Core 0), essential components are set up, including the serial connection, CSV logging file, TensorFlow model, and real-time plotting functions. It also monitors system tasks such as CPU and RAM usage, temperature, and latency, while updating real-time ECG data plots, including scalogram representations and prediction results. Following this, Core 1 is dedicated to data acquisition, reading data through the serial interface at a 115200 baud rate and storing it in a queue. This non-blocking, efficient approach ensures continuous data flow without delays. Subsequently, Core 2 handles data processing tasks, particularly CWT conversion and image generation for the classification model. Once a sufficient batch of 10 PQRST samples is collected in the queue, Core 2 transforms the 1D ECG signal from the temporal domain into a 2D frequency-time representation using the selected wavelet. This scalogram image is then saved and prepared for classification using the TensorFlow Lite model to predict the ECG status, distinguishing normal signals from those with specific anomalies. The core displays the prediction along with an associated message in real-time on the dashboard. Moreover, the system dynamically checks core availability to optimize performance, offloading computation heavy tasks such as CWT conversion and classification, to other cores when possible along with logging the performance metrics of each task from data acquisition to prediction. Finally, ECG data and corresponding predictions are saved in CSV files.

⁵ <https://developer.nvidia.com/embedded/learn/get-started-jetson-nano-devkit>

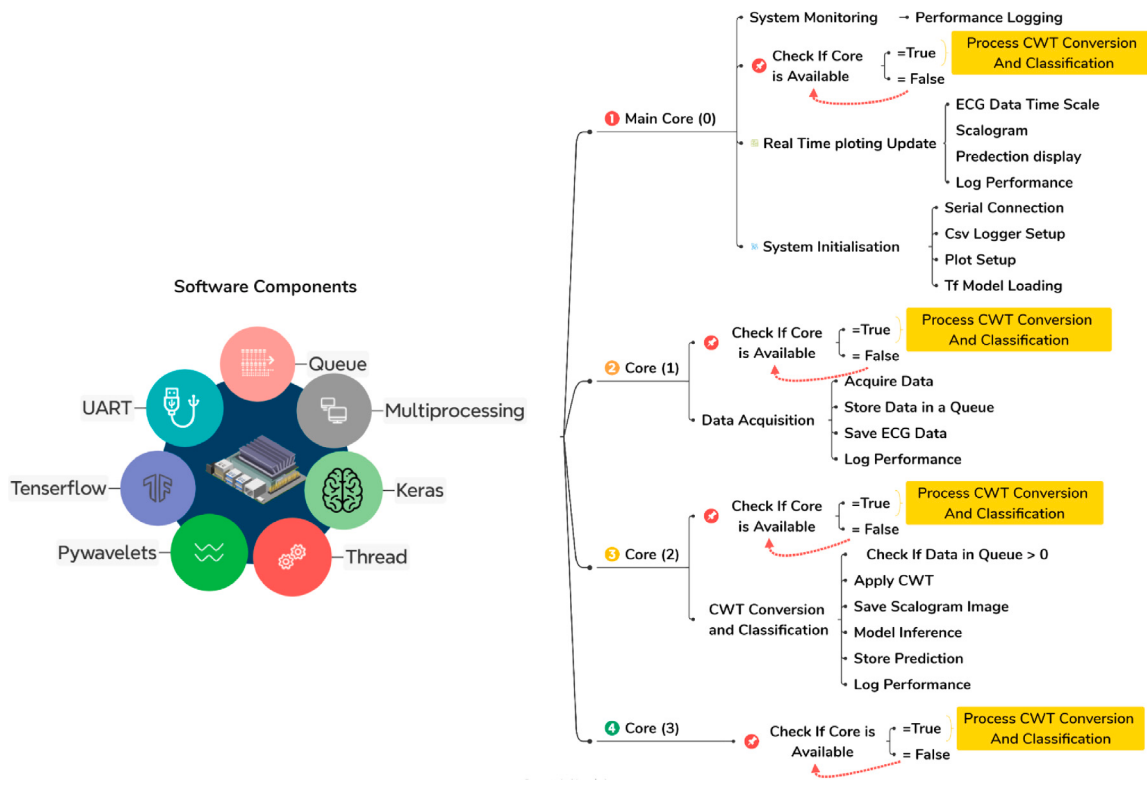


Fig. 6. System architecture workflow.

for easy access and processing, while generated scalograms are stored as images in a designated folder for later evaluation and review. This architecture minimizes resource contention, creating a robust, real-time ECG diagnostic system that provides immediate feedback on signal quality, aiding medical staff in accelerating the diagnostic process.

4. Results and discussion

This section presents and discusses the optimal TL performance for ECG diagnosis, focusing on which wavelet provides the best results in terms of feature extraction. Additionally, it analyzes the overall performance of the real-time system after deployment onto the hardware, evaluating multiple factors such as latency, processor load, required resources, and energy consumption.

4.1. Assessing model performance

To evaluate model performance and identify the optimal wavelet, we conducted a comparative analysis across the two datasets, the results of which are presented in two tables. Each table displays key performance metrics for various wavelet selections and models. Additionally, each table corresponds to a specific (L_r) of the Adam optimizer, set at 10^{-3} and 10^{-4} , respectively.

According to Table 3, the CMOR and MEXH wavelets demonstrate outstanding performance on the SNIR dataset. Across all models, metrics consistently reached 100%, with exceptionally low loss values; notably with V19 model that achieved a minimal loss of just 0.0001. When evaluated on the PTB dataset, the V19 model also excelled, surpassing other models by achieving 100% in precision, recall, and F-score, alongside an accuracy of 99.84% and a minimal loss of 0.0087 using the CMOR wavelet. As well, when using the MEXH wavelet, the V19 model attained an accuracy of 99.3%, with other metrics at 99% and a loss of 0.0275. In contrast, the SHAN wavelet produced considerably lower performance metrics compared to CMOR and MEXH, despite that, the V19 model continues to achieve the best performance.

Consistent on Table 4, and in liaison with a L_r of 10^{-4} exploring the CMOR wavelet for the SNIR and PTB datasets, both V16 and V19 models demonstrated exceptional performance across all metrics, with V19 slightly outperforming V16. When switching to the MEXH wavelet, the Inv3, Xce, V19, and Efb0 models achieved 100% across all metrics on the SNIR dataset. However, on the PTB dataset, V19 continued to excel, reaching 99% in p, F, and R, with an A of 99.61% and a slightly higher loss of 0.0179, surpassing the other models. Additionally, the SHAN wavelet showed improved results compared to the previous L_r but still underperformed relative to the other wavelets.

Based on these results, we identify that the combination of the CMOR wavelet with the V19 model offers the optimal configuration across both datasets and various L_r . To further illustrate the impact of L_r on model training stability particularly in terms of convergence and overfitting, we present the ROC curves for this optimal configuration under different L_r settings in Fig. 7.

Figs. 7 reveal that peak model performance and stabilization were generally achieved after 30 epochs. Notably, training and validation curves with a L_r of 10^{-3} showed signs of instability, suggesting potential overfitting despite strong final metrics. In contrast, a L_r of 10^{-4} exhibited consistent and stable behavior throughout the epochs, indicating more effective training and enhanced robustness.

The results indicate that CMOR and MEXH wavelets demonstrated strong performance across different TL models, delivering near perfect performance metrics on both the SNIR and PTB datasets. Moreover, MEXH exhibited greater sensitivity to learning rate (L_r) adjustments compared to CMOR, suggesting that careful tuning of L_r is necessary to avoid performance degradation. Conversely, the SHAN wavelet displayed significant variability, particularly at higher L_r values, where key metrics fell below the desired threshold. This inconsistency suggests that the SHAN wavelet may be less suitable for applications requiring high accuracy and stability. As well these insights confirm CMOR as a highly reliable choice for robust ECG analysis, supporting the hypothesis discussed in Section 3.2.2, where it was shown that this wavelet provides superior performance. Additionally, among the TL

Table 3Metrics evaluation across different wavelets and TL models on both datasets with $Lr = 10^{-3}$.

Wavelet	Model	NSIR					PTB				
		P (%)	A (%)	F (%)	R (%)	L (%)	P (%)	A (%)	F (%)	R (%)	L (%)
CMOR	Inv3	100	100	100	100	0.0003	97	95.93	94	91	0.1180
	Xce	100	100	100	100	0.0047	94	93.83	92	90	0.1665
	V16	100	100	100	100	0.0003	99	98.20	99	98	0.0334
	V19	100	100	100	100	0.0001	100	99.84	100	100	0.0087
	Efb0	100	100	100	100	0.0038	95	96.33	96	97	0.0973
MEXH	Inv3	100	100	100	100	0.0003	97	95.93	94	91	0.1180
	Xce	100	100	100	100	0.0114	86	89.06	88	91	0.2420
	V16	100	100	100	100	0.0002	99	98.30	99	99	0.0275
	V19	100	100	100	100	0.0001	99	99.91	99	99	0.0255
	Efb0	100	100	100	100	0.0006	95	97.81	96	96	0.0669
SHAN	Inv3	94.51	94	92.01	90	0.1012	87	90	90	90.1	0.4660
	Xce	90	92.45	92.47	89	0.1232	85.4	84.28	77	77	0.5461
	V16	94	92.4	89	87.5	0.2153	90	92.73	88.2	84	0.3590
	V19	96	94.3	92	89	0.1015	94	92.97	89.6	86	0.2185
	Efb0	89	90.1	83.4	91	0.3120	78	81.75	79	88	0.5138

Table 4Metrics evaluation across different wavelets and TL models on both datasets with $Lr = 10^{-4}$.

Wavelet	Model	NSIR					PTB				
		P (%)	A (%)	F (%)	R (%)	L (%)	P (%)	A (%)	F (%)	R (%)	L (%)
CMOR	Inv3	99	99.33	99	99	0.0274	98	97.66	98	97	0.0675
	Xce	99	98.66	99	99	0.0562	91	84.38	74	71	0.4662
	V16	100	100	100	100	0.0232	99	99.30	99	99	0.0225
	V19	100	100	100	100	0.0107	99	99.61	99	99	0.0179
	Efb0	99	99.33	99	99	0.0411	98	97.81	97	97	0.0625
MEXH	Inv3	100	100	100	100	0.0039	97	98.63	97	98	0.0508
	Xce	100	100	100	100	0.0260	97	95.63	94	92	0.1012
	V16	99	99.33	99	99	0.0263	99	98.83	99	98	0.0362
	V19	100	100	100	100	0.0284	99	99.22	99	99	0.0243
	Efb0	100	100	100	100	0.0264	98	98.36	98	98	0.0515
SHAN	Inv3	100	100	100	100	0.0185	92	94.77	98	93	0.1341
	Xce	100	100	100	100	0.0282	92	93.63	91	90	0.1752
	V16	97	97.32	97	98	0.0558	97	97.73	98	98	0.0644
	V19	99	99.33	99	99	0.0414	99	98.36	99	99	0.0492
	Efb0	100	100	100	100	0.0592	90	93.91	92	95	0.1394

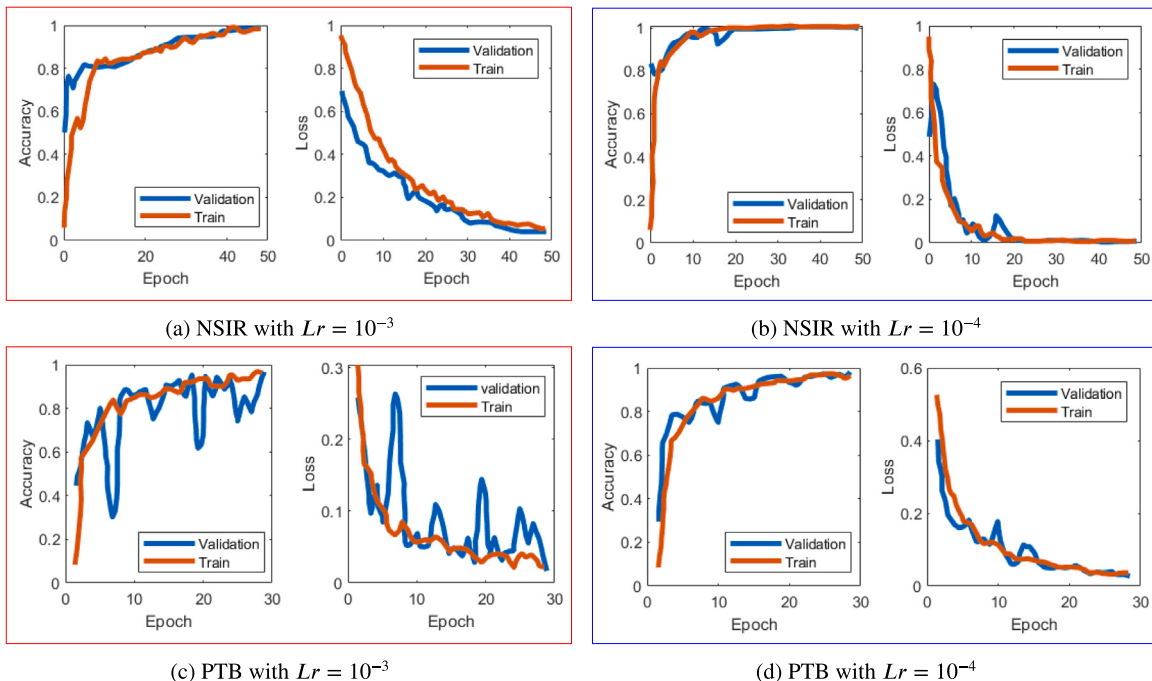
**Fig. 7.** ROC curves using CMOR wavelet with v19 model across different Lr with (a) present NSIR dataset with $Lr = 10^{-3}$, (b) NSIR dataset with $Lr = 10^{-4}$, (c) PTB dataset with $Lr = 10^{-3}$ and (d) PTB dataset with $Lr = 10^{-4}$.



Fig. 8. Hardware materials and tools.

models, V19 consistently achieved the best metrics across datasets, making it the optimal choice. It also requires a smaller input image size, offering the advantage of reduced memory usage when storing data. Besides L_r Adjustment directly influences the training process, and fine-tuning it based on the progression of loss and accuracy which can help avoid overfitting and ensure a more robust model with lower loss.

4.2. Model deployment and evaluation

After identifying the optimal wavelet and finalizing the best model, the system architecture is established, marking the beginning of the deployment phase. This starts with configuring the Linux Ubuntu 20.04 operating system on a 64 GB SD card, followed by installing essential software, including TensorRT 8.0.1.6, CUDA 10.2, and additional necessary packages. Once the environment setup is complete, the system structure is executed within Visual Studio to verify the software configuration. Upon successful software verification we move to hardware connections to initiate the overall system performance testing. Test performance will be conducted on the two datasets, starting with SNIR and then moving to PTB.

4.2.1. Test conducted with SNIR dataset

The test scenario was conducted on a healthy female volunteer with no known heart diseases. We began by applying the acquisition protocol, which includes cleaning the orbital SilverBumps® (OR90) electrodes and the intended placement area with alcohol. Next, the electrodes were placed based on three configurations to acquire a clean ECG signal. External influences were then applied to introduce 50/60 Hz power line interference and electrode placement artifacts, in order to assess the system's recognition capabilities. Fig. 8 presents the hardware system with all necessary tools, as well as Fig. 9 illustrates the output of the actual test conducted on the subject along with the predictions, where each class is identified through its corresponding scalogram representation.

4.2.2. Test conducted with PTB dataset

Test conducted on the PTB dataset does not include data acquisition with the electrode. Instead, signals will be delivered as a matrix initialized on the STM32 for further processing in the next steps, Fig. 10 display classification output.

4.2.3. Hardware monitoring

Aiming to monitor the system's hardware resource requirements and time consumption while implementing the V19 model using the cmor wavelet Table 5 presents performance metrics logged at each stage. Including functions latency, per-core CPU usage, RAM consumption and the temperature of the Jetson Nano.

The overall performance of the Jetson Nano board during the execution of real time ECG signal processing tasks demonstrates effective resource utilization, with efficient management of CPU parallelism and execution time across all tasks. The Serial Acquisition and Plot Update tasks are performed seamlessly, while CWT Conversion and Classification push the CPU to its limits due to the computationally intensive nature of wavelet transformations. The balanced core usage and consistent temperature readings indicate that the Jetson Nano manages the workloads well without risking system damage. However, when comparing the CWT stage across different datasets, the PTB dataset introduces significantly higher latency and RAM usage. This is primarily due to the presence of diseased ECG signals, which exhibit greater morphological variations, abrupt changes, and increased noise levels. These pathological irregularities require more computation for accurate wavelet decomposition as they introduce non stationary features. Additionally, diseased ECG signals often contain higher frequency components, further increasing the computational load when performing CWT at multiple scales. Even so, for more demanding and advanced applications, a more powerful board with an enhanced GPU would ensure smoother processing with improved reliability. Upgrading to a Jetson Xavier or Orin, with higher computational resources and superior GPU acceleration, would mitigate system strain and enable efficient handling of computationally heavy tasks such as wavelet transformations, ensuring real-time performance without the risk of system overload or processing delays.

4.2.4. Comparison with existing works

In order to validate our results and demonstrate their high potential feasibility and applicability, Table 6 presents a comprehensive comparison with existing research, focusing on electrode types, explored dataset, AI/model types, feature extraction techniques, accuracy, and deployment platforms.

While wet electrodes are traditionally preferred in ECG studies, this research demonstrates that dry electrodes offer significant improvements in user comfort while providing signal quality comparable to wet electrodes, without the need for conductive gels. Analysis of the AI models reveals that the proposed system, which incorporates V19 with CWT scalogram feature extraction, achieved (100%-99.661%) accuracy in software evaluations respectively on appropriate dataset

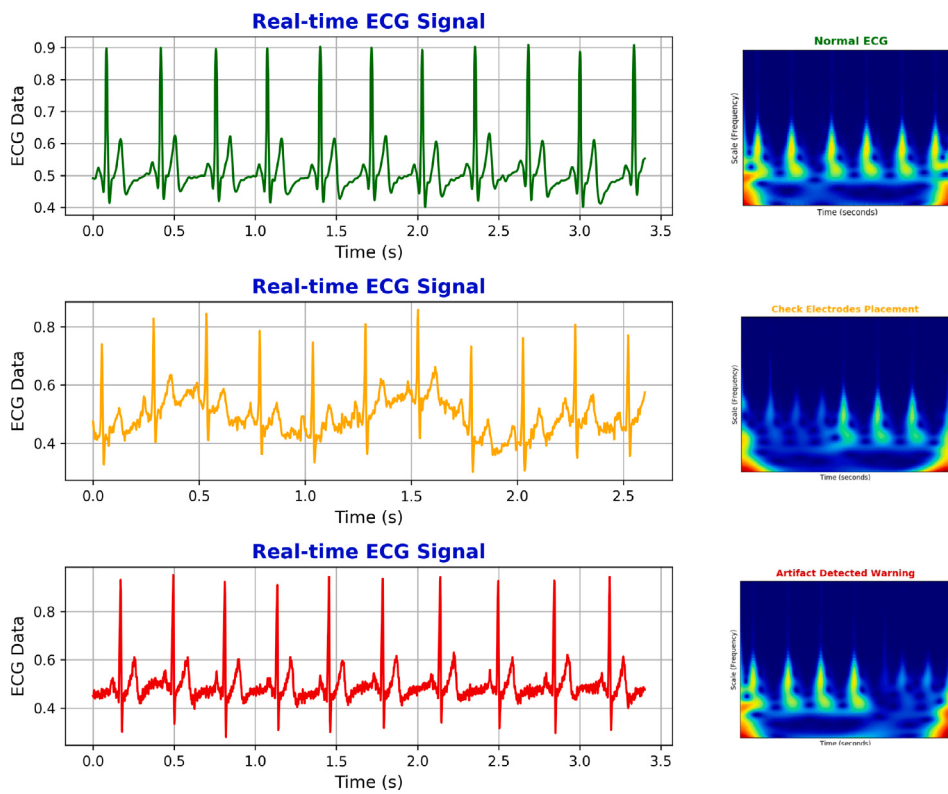


Fig. 9. Classification test using NSIR dataset and the designed system along with output prediction.

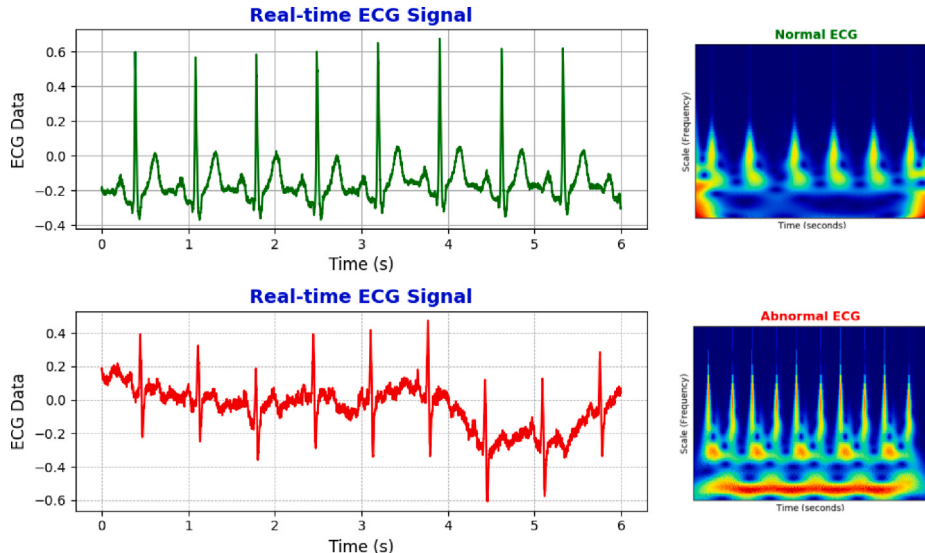


Fig. 10. Classification test using PTB dataset and the designed system along with output prediction.

Table 5
Resource hardware monitoring.

Dataset	Executed task	Latency (ms)	Core Usage (%)	RAM Usage (%)	Temperature (°C)
SNIR	Serial Acquisition	0.715	[54.5, 62.5, 88.9, 77.8]	64	37.5
	CWT Conversion and Classification	1.192	[99.3, 99.1, 99.8, 98.8]	67.7	40
	Plot Update	0.477	[100.0, 100.0, 0.0, 0.0]	64.6	38
PTB	Serial Acquisition	0.715	[50.0, 100.0, 0.0, 0.0]	57.3	39.5
	CWT Conversion and Classification	2.86	[99.7, 99.7, 99.6, 99.5]	76.3	41.75
	Plot Update	0.477	[100.0, 0.0, 0.0, 100.0]	57.7	39.75

Table 6

Comparative study of ECG classification and anomaly detection methods.

Ref	Electrode type	Dataset	AI/Model	Feature extraction	A (%)	Deployment
[52]	Wet Electrodes	MIT BIH	i-AlexNet CNN	Red Fox optimization	98.80	Software
[53]	Wet Electrodes	PTB	RCNN	Gray Wolf Optimization (GWO)	98.00	Software
[54]	Wet Electrodes	PTB-XL	GRU-LSTM	1D and 2D-CNN	81.04	Software
[55]	Wet Electrodes	MIT-BIH	MLP	DWT	98.30	Software
[56]	Textile Dry Electrodes	PhysioNet Challenge 2017	Transformer	CWT	97.20	Software
[57]	Embroidered Dry Electrodes	Private	polynomial regression	Temporal features	94.90	Software
Our system	Or90 Dry Electrodes	SNIR	V19	CWT	100	Software
Our system	Or90 Dry Electrodes	PTB	V19	CWT	99.61	Software
[58]	Wet Electrodes	PTB-XL	CNN-LSTM	Not specified	81.21	Raspberry Pi
[59]	Wet Electrodes	MIT BiH	Supreme CNN	1D-CNN	97.34	FPGA (ZCU106)
[55]	Wet Electrodes	MIT-BIH	MLP	DWT	95.00	FPGA (NEXYS4)
[60]	Wearable Dry Electrodes	Private	Cross-Modal Learning	variational autoencoder(VAE)	98.82	FPGA
Our system	Or90 Dry Electrodes	SNIR	V19	CWT	99.87	Jetson Nano
Our system	Or90 Dry Electrodes	PTB	V19	CWT	99.30	Jetson Nano

and the public ptb dataset with its large variety of diseases, outperforming other models. further along hardware evaluation, the model maintained an impressive (99.87%–99.3%) performance, the highest among hardware based systems. This approach effectively combines TL and CWT, extracting critical temporal and frequency domain information necessary for precise anomaly detection. Furthermore, the Jetson Nano's computational capabilities facilitate real-time processing with efficient energy usage, It operates on a standard 5 V power supply with a recommended current capacity up to 4 A, making it ideal for embedded healthcare applications.

These findings indicate that dry electrodes, combined with advanced feature extraction techniques and optimized hardware, offer a promising solution for real-time, high performance ECG diagnostic assistance system, This system could serve as a reliable diagnostic tool in clinical settings, particularly in ambulatory and telemedicine scenarios. The 2D graphical representation of the ECG signals ensures precise interpretation and reduces the risk of misunderstanding of the heart state.

4.3. Limitations

The current study has certain limitations that must be acknowledged. The system relies solely on a single lead ECG signal, which may not provide as comprehensive a view of cardiac activity as multi lead systems. Additionally, hardware anomaly detection and disease detection are handled separately, which could be optimized by integrating them into a single model for improved efficiency. The embedded board, with only 4 GB of RAM, also limits prolonged monitoring and high frequency data processing. Lastly, while the SNIR dataset is effective for validation, its expansion is necessary to enhance the generalizability of our findings.

5. Conclusion

This study introduces a pioneering approach to real-time ECG anomaly detection, addressing limitations in traditional cardiac monitoring systems by integrating dry electrodes, TL and CWT techniques. By utilizing Orbital dry electrodes, the system alleviates common issues of skin irritation and signal degradation typically associated with wet electrodes, ensuring comfort and consistent signal quality during extended monitoring. This makes it particularly suitable for continuous, non-invasive cardiac assessments.

The ECG acquisition and signal processing setup leverages STM32 microcontrollers and the AD8232 module, effectively capturing high-fidelity signals while minimizing artifacts, thereby supporting accurate diagnostics, focal point of this research lies in transforming ECG signals into scalogram images using CWT with various wavelet (CMOR, MEXH, and SHAN). Among these, the CMOR wavelet demonstrated a superior balance between high- and low-frequency ECG features, essential for robust anomaly detection.

This paper rigorously evaluated multiple TL models (InV3, V16, V19, Xpe and Efb0), finding that V19 paired with the CMOR wavelet achieved optimal classification accuracy, reaching up to 100% with a $Lr = 10-4$. Additionally, the system's deployment on an NVIDIA Jetson Nano platform provided up to 99.87% accuracy with efficient, low-latency real-time processing, utilizing multithreading and parallel core allocation to enhance resource utilization and task execution. This hardware setup effectively balances accuracy and responsiveness, fulfilling the demands of real-time diagnostic applications.

Comparative analysis with other studies underscores this system's competitive accuracy and adaptability for embedded platforms, emphasizing its potential in cardiac health assistance devices. Future developments would focus on several key areas to enhance the system's performance and usability. Such as the investigation of the impact of varying learning rates on the training stability. The exploration of multiple ECG leads to increase diagnostic accuracy and upgrade the system to advanced platforms, such as the Jetson Xavier, to perform concurrently dual tasks. Further advancements will include the exploration of innovative and comfortable textile based dry electrodes. Also the system validation tests will cover a wider range of cardiac conditions and environmental factors. Finally, the integration of a Wi-Fi-enabled interactive platform will allow efficient data synchronization with cloud services, to support effective remote monitoring capabilities.

Ultimately, this research establishes a robust framework for high-accuracy, real-time ECG monitoring in compact, non-invasive formats, laying a solid foundation for advancements in accessible and reliable cardiac diagnostic assistance systems.

CRediT authorship contribution statement

Wissem Kharzi: Writing – review & editing, Writing – original draft, Software, Resources, Project administration, Methodology, Investigation, Funding acquisition, Formal analysis, Data curation, Conceptualization. **Nacera Meziane:** Writing – review & editing, Visualization, Validation, Supervision. **Hadjer Zairi:** Writing – review & editing, Visualization, Validation, Supervision. **Malika Kedir Talha:** Writing – review & editing, Visualization, Validation, Supervision. **Lotfi Madaoui:** Writing – review & editing, Visualization, Validation, Supervision. **Oussama Kerdjidj:** Writing – review & editing, Visualization, Validation, Supervision.

Declaration of competing interest

The authors declare that they have no known competing financial interests or personal relationships that could have appeared to influence the work reported in this paper.

Acknowledgment

This research was supported from the Ministry of Higher Education and Scientific Research (MESRS) of the Algerian Government.

Data availability

Data will be made available on request.

References

- [1] C. Qiu, H. Li, C. Qi, B. Li, Enhancing ECG classification with continuous wavelet transform and multi-branch transformer, *Heliyon* (2024).
- [2] K. Meddah, M. Kedir Talha, M. Bahoura, H. Zairi, FPGA-based system for heart rate monitoring, *IET Circuits, Devices Syst.* 13 (6) (2019) 771–782.
- [3] S. Somani, A.J. Russak, F. Richter, S. Zhao, A. Vaid, F. Chaudhry, J.K. De Freitas, N. Naik, R. Miotto, G.N. Nadkarni, et al., Deep learning and the electrocardiogram: review of the current state-of-the-art, *EP Eur.* 23 (8) (2021) 1179–1191.
- [4] C.H. Lee, S.H. Kim, ECG measurement system for vehicle implementation and heart disease classification using machine learning, *IEEE Access* 11 (2023) 17968–17982.
- [5] N. Meziane, D. Meziane, M. Bouzid, Discrete wavelet transform-based denoising method for real electrocardiogram, in: 2023 International Conference on Smart Applications, Communications and Networking, SmartNets, IEEE, 2023, pp. 1–5.
- [6] J. Schläpfer, H.J. Wellens, Computer-interpreted electrocardiograms: benefits and limitations, *J. Am. Coll. Cardiol.* 70 (9) (2017) 1183–1192.
- [7] G.A. Roth, G.A. Mensah, C.O. Johnson, G. Addolorato, E. Ammirati, L.M. Baddour, N.C. Barengo, A.Z. Beaton, E.J. Benjamin, C.P. Benziger, et al., Global burden of cardiovascular diseases and risk factors, 1990–2019: update from the GBD 2019 study, *J. Am. Coll. Cardiol.* 76 (25) (2020) 2982–3021.
- [8] S. Din, M. Qaraqe, O. Mourad, K. Qaraqe, E. Serpedin, ECG-based cardiac arrhythmias detection through ensemble learning and fusion of deep spatial-temporal and long-range dependency features, *Artif. Intell. Med.* (2024) 102818.
- [9] N. Meziane, S. Yang, M. Shokoueinejad, J. Webster, M. Attari, H. Eren, Simultaneous comparison of 1 gel with 4 dry electrode types for electrocardiography, *Physiol. Meas.* 36 (3) (2015) 513.
- [10] W. Kharzi, N. Meziane, M.-D. Kedir-Talha, Towards the exploration of dry electrodes performance in bioimpedance measurements based on the AD5933 chip, in: 2023 2nd International Conference on Electronics, Energy and Measurement (IC2EM), vol. 1, IEEE, 2023, pp. 1–7.
- [11] M.K. Gajendran, M.Z. Khan, M.A.K. Khattak, Ecg classification using deep transfer learning, in: 2021 4th International Conference on Information and Computer Technologies, ICICT, IEEE, 2021, pp. 1–5.
- [12] R.S. Salles, P.F. Ribeiro, The use of deep learning and 2-D wavelet scalograms for power quality disturbances classification, *Electr. Power Syst. Res.* 214 (2023) 108834.
- [13] O. Kerdjidj, Y. Himeur, S. Atalla, A. Copiaco, A. Amira, F. Fadli, S.S. Sohail, W. Mansoor, A. Gawanmeh, S. Miniaoui, Exploiting 2D representations for enhanced indoor localization: A transfer learning approach, *IEEE Sens. J.* (2024).
- [14] J. Guo, X. Wang, R. Bai, Z. Zhang, H. Chen, K. Xue, C. Ma, D. Zang, E. Yin, K. Gao, et al., A cost-effective and easy-to-fabricate conductive velcro dry electrode for durable and high-performance biopotential acquisition, *Biosensors* 14 (9) (2024) 432.
- [15] R. Al-Haidari, B. Falola, M. Alhendi, M.J. Schadt, M. Poliks, D. Balder, A. Stemmermann, M. Foster, V. Balchand, T.-J. Kao, et al., Conformal dry electrode for ECG monitoring, in: 2024 IEEE 74th Electronic Components and Technology Conference, ECTC, IEEE, 2024, pp. 1662–1669.
- [16] A. Abdou, S. Krishnan, ECG dry-electrode 3D printing and signal quality considerations, in: 2021 43rd Annual International Conference of the IEEE Engineering in Medicine & Biology Society, EMBC, IEEE, 2021, pp. 6855–6858.
- [17] A. Abdou, S. Krishnan, ECG dry electrodes design and analysis, in: Advances in 3D Bioprinting, CRC Press, 2023, pp. 195–214.
- [18] F. Wang, W. Yao, B. Liu, R. Fu, ECG-based real-time drivers' fatigue detection using a novel elastic dry electrode, *IEEE Trans. Instrum. Meas.* (2023).
- [19] A. Joutsen, A. Cömert, E. Kaappa, K. Vanhatalo, J. Riistama, A. Vehkaoja, H. Eskola, ECG signal quality in intermittent long-term dry electrode recordings with controlled motion artifacts, *Sci. Rep.* 14 (1) (2024) 8882.
- [20] P. Laferriere, E.D. Lemaire, A.D. Chan, Surface electromyographic signals using dry electrodes, *IEEE Trans. Instrum. Meas.* 60 (10) (2011) 3259–3268.
- [21] W. Kharzi, N. Meziane, M.-D. Kedir-Talha, A low cost bioimpedance measurement system based on AD5933 chip, in: 2023 International Conference on Decision Aid Sciences and Applications, DASA, IEEE, 2023, pp. 198–202.
- [22] A.M. Abagaro, H. Barki, G. Ayana, A.A. Dawud, B.L. Thamineni, T. Jemal, S.-w. Choe, Automated ECG signals analysis for cardiac abnormality detection and classification, *J. Electr. Eng. Technol.* (2024) 1–17.
- [23] S.R. Marwa, M.A. Shakir, Improving ECG signals classification by using deep learning techniques: A review, in: ITM Web of Conferences, vol. 64, EDP Sciences, 2024, p. 01023.
- [24] R. Vavekanand, K. Sam, S. Kumar, T. Kumar, CardiacNet: A neural networks based heartbeat classifications using ECG signals, *Stud. Med. Heal. Sci.* 1 (2) (2024) 1–17.
- [25] M. Maleki, Identification of cardiovascular diseases through ECG classification using wavelet transformation, 2024, arXiv preprint [arXiv:2404.09393](https://arxiv.org/abs/2404.09393).
- [26] V.D. Kota, H. Sharma, M.V. Albert, I. Mahbub, G. Mehta, K. Namuduri, A low-power wireless system for predicting early signs of sudden cardiac arrest incorporating an optimized CNN model implemented on NVIDIA jetson, *Sensors* 23 (4) (2023) 2270.
- [27] D. Lee, S. Lee, D. Park, FPGA-based cloudification of ECG signal diagnosis acceleration, in: 2021 Twelfth International Conference on Ubiquitous and Future Networks, ICUFN, IEEE, 2021, pp. 236–238.
- [28] E.S. Pramukantoro, K. Amron, V. Wardhani, P.A. Kamila, Comparative analysis of classification features for ECG signal classification on Raspberry Pi using wearable sensor data, in: Proceedings of the 8th International Conference on Sustainable Information Engineering and Technology, 2023, pp. 612–618.
- [29] L. Mhamdi, O. Dammak, F. Cottin, I. Ben Dhaou, Deep learning for COVID-19 contamination analysis and prediction using ECG images on Raspberry Pi 4, *Int. J. Imaging Syst. Technol.* 33 (6) (2023) 1858–1869.
- [30] O.R. Inc., SilverBumps® electrodes, 2020, URL chrome-extension: //efaidnbmnnpibpcajpcglclefimdmkj/https://www.orbitalresearch.com/Specification%20Sheets/SilverBumps_Electrodes_Brochure_rev15_2020.pdf. (Accessed 7 August 2024).
- [31] N. Meziane, M. Bouzid, D. Meziane, Cardiovascular monitoring system using android-based mobile application with cloud firebase, in: 2023 International Conference on Decision Aid Sciences and Applications, DASA, IEEE, 2023, pp. 203–207.
- [32] V.A. Ardeti, V.R. Kolluru, S. Routray, B.O.L. Jagan, A.K. Kumar, R. Ramachandran, M.A. Hossain, A.N.Z. Rashed, Development of real time ECG monitoring and unsupervised learning classification framework for cardiovascular diagnosis, *Biomed. Signal Process. Control.* 88 (2024) 105553.
- [33] R.I. Darmawan, A. Surtono, D.K. Apriyanto, A. Supriyanto, Design of computer based 12 lead ECG using STM32F401 microcontroller, *J. Energy, Mater. Instrum. Technol.* 3 (4) (2022) 147–156.
- [34] Y.-p. Su, Design of ECG acquisition and display system based on ADS1292r and STM32 microcontroller, in: 2022 15th International Congress on Image and Signal Processing, BioMedical Engineering and Informatics, CISB-BMEI, IEEE, 2022, pp. 1–5.
- [35] R. Bousseljot, D. Kreiseler, A. Schnabel, Nutzung der EKG-Signaldatenbank CARDIODAT der PTB über das Internet, Walter de Gruyter, Berlin/New York Berlin, New York, 1995.
- [36] M. Kachuee, S. Fazeli, M. Sarrafzadeh, Ecg heartbeat classification: A deep transferable representation, in: 2018 IEEE International Conference on Healthcare Informatics, ICHI, IEEE, 2018, pp. 443–444.
- [37] W. Kharzi, O. Kerdjidj, N. Meziane, M.-D. Kedir-Talha, L. Madaoui, H. Zairi, Dry ECG Dataset: Normal-Recorded Signals and Interference-Affected Records, Zenodo, 2024, <http://dx.doi.org/10.5281/zenodo.13147251>.
- [38] F. Demir, V. Bajaj, M.C. Ince, S. Taran, A. Şengür, Surface EMG signals and deep transfer learning-based physical action classification, *Neural Comput. Appl.* 31 (2019) 8455–8462.
- [39] H. Khorrami, M. Moavenian, A comparative study of DWT, CWT and DCT transformations in ECG arrhythmias classification, *Expert Syst. Appl.* 37 (8) (2010) 5751–5757.
- [40] S. Alghanemi, H. Almisbah, E. Alkayal, Enhancing multivariate time series forecasting accuracy through integration of CWT scalograms as CNN channels, in: Innovative and Intelligent Digital Technologies: Towards an Increased Efficiency: Volume 2, Springer, 2025, pp. 37–48.
- [41] G. Serbes, Robust spike sorting using dual tree complex wavelet transform: Overcoming traditional limitations, *IEEE Access* (2024).
- [42] W.K. Ngui, M.S. Leong, L.M. Hee, A.M. Abdelrhman, Wavelet analysis: mother wavelet selection methods, *Appl. Mech. Mater.* 393 (2013) 953–958.
- [43] J. Xie, W. Chen, H. Dai, Distributed cooperative learning algorithms using wavelet neural network, *Neural Comput. Appl.* 31 (2019) 1007–1021.
- [44] Q. Yu, Q. Guan, P. Li, T.-B. Liu, J.-F. Si, Y. Zhao, H.-X. Liu, Y.-Q. Wang, Wavelet optimization for applying continuous wavelet transform to maternal electrocardiogram component enhancing, *Chin. Phys. B* 26 (11) (2017) 118702.
- [45] M. Aqil, A. Jbari, Continuous wavelet analysis and extraction of ECG features, *Emerg. Technol. Biomed. Eng. Sustain. TeleMedicine* (2021) 51–68.
- [46] Y. Lin, H. Zhang, W. Wu, X. Gao, F. Chao, J. Lin, Wavelet transform and deep learning-based obstructive sleep apnea detection from single-lead ECG signals, *Phys. Eng. Sci. Med.* 47 (1) (2024) 119–133.
- [47] F. Zhuang, Z. Qi, K. Duan, D. Xi, Y. Zhu, H. Zhu, H. Xiong, Q. He, A comprehensive survey on transfer learning, *Proc. IEEE* 109 (1) (2020) 43–76.
- [48] C. Szegedy, V. Vanhoucke, S. Ioffe, J. Shlens, Z. Wojna, Rethinking the inception architecture for computer vision, in: Proceedings of the IEEE Conference on Computer Vision and Pattern Recognition, 2016, pp. 2818–2826.
- [49] F. Chollet, Xception: Deep learning with depthwise separable convolutions, in: Proceedings of the IEEE Conference on Computer Vision and Pattern Recognition, 2017, pp. 1251–1258.
- [50] K. Simonyan, A. Zisserman, Very deep convolutional networks for large-scale image recognition, 2014, arXiv preprint [arXiv:1409.1556](https://arxiv.org/abs/1409.1556).
- [51] M. Tan, Q. Le, Efficientnet: Rethinking model scaling for convolutional neural networks, in: International Conference on Machine Learning, PMLR, 2019, pp. 6105–6114.

- [52] M. Kolhar, R.N.A. Kazi, H. Mohapatra, A.M. Al Rajeh, AI-driven real-time classification of ECG signals for cardiac monitoring using i-AlexNet architecture, *Diagnostics* 14 (13) (2024) 1344.
- [53] P.N. Singh, R.P. Mahapatra, A novel deep learning approach for arrhythmia prediction on ECG classification using recurrent CNN with GWO, *Int. J. Inf. Technol.* 16 (1) (2024) 577–585.
- [54] H. Narotamo, M. Dias, R. Santos, A.V. Carreiro, H. Gamboa, M. Silveira, Deep learning for ECG classification: A comparative study of 1D and 2D representations and multimodal fusion approaches, *Biomed. Signal Process. Control.* 93 (2024) 106141.
- [55] H. Zairi, M. Kedir Talha, K. Meddah, S. Ould Slimane, FPGA-based system for artificial neural network arrhythmia classification, *Neural Comput. Appl.* 32 (2020) 4105–4120.
- [56] A.H. Ribeiro, et al., Automatic diagnosis of the 12-lead ECG using a deep neural network, *Nat. Commun.* 11 (1) (2020) 1760.
- [57] G.B. Othman, A.A. Kumar, F.B. Hassine, D. Copot, L. Sidhom, E.N. Kamavuako, M. Trabelsi, C.M. Ionescu, I. Chihi, Sustainability and predictive accuracy evaluation of gel and embroidered electrodes for ECG monitoring, *Biomed. Signal Process. Control.* 96 (2024) 106632.
- [58] K. Sharma, R. Eskicioglu, Deep learning-based ECG classification on raspberry PI using a tensorflow lite model based on PTB-XL dataset, 2022, arXiv preprint arXiv:2209.00989.
- [59] V. Rawal, P. Prajapati, A. Darji, Hardware implementation of 1D-CNN architecture for ECG arrhythmia classification, *Biomed. Signal Process. Control.* 85 (2023) 104865.
- [60] N.R. Vora, Exploring machine learning techniques for embedded hardware, 2024.